JOURNAL OF MATERIALS SCIENCE 29 (1994) 1417–1435

Characterization of boron nitride films deposited from BCl_3–NH_3–H_2 mixtures in chemical vapour infiltration conditions

V. CHOLET, L. VANDENBULCKE, J.P. ROUAN
LCSR-CNRS, 45071 Orléans Cedex 2, France

P. BAILLIF
University of Orléans, ESEM, 45067 Orléans, France

R. ERRE
CRMD-CNRS, 45071 Orléans Cedex 2, France

Boron nitride (BN) thin films deposited by isopressure and isothermal chemical vapour infiltration (ICVI) from BCl_3–NH_3–N_2 mixtures have been characterized from a physico-chemical point of view as functions of both the deposition conditions and the destabilizing action of moisture. As-deposited (deposited at 773 K and post-treated at 1273 K), the BN films are turbostractic ($d_{0\,0\,2}=0.36$ nm, $L_c=1.5$ nm), have a low density (1.4 g cm^{-3}) and contain oxygen (about 20 at%). A first oxygen content (191.5 eV by XPS) is inserted in the films during the CVI step in relation to the hygroscopy of intermediate solid products and the quasi-equilibrium between the formation of BN and B_2O_3. A second oxygen content (192.5 eV) is due to the hydrolysis of BN by moisture which induces a very drastic transformation of BN. This destabilization affects both boron and nitrogen atoms and leads to the formation of ammonium borate hydrates. Different post-treatments have been investigated to stabilize the BN films and it appears that nitriding under ammonia is the most efficient.

1. Introduction

Chemical vapour deposition (CVD) of boron nitride (BN) has been widely investigated for many years, because of the numerous properties associated with bulk boron nitride and also the ease of production of pure boron nitride by CVD techniques [1]. Boron nitride has similar crystalline structures to carbon, which leads to similar properties, except that BN has a high electrical resistivity, particularly at high temperature [2]. As in the case of carbon, the thermal CVD techniques allow deposition of hexagonal BN or derived forms (turbostratic or amorphous) [4–6], while the deposition of cubic BN would necessitate the association of an external excitation source (plasma, ion beam or hot filament); however, the deposition of well-crystallized cubic BN has never proved to be obtained by these techniques, contrary to diamond [7].

While ammonia has generally been the gaseous precursor of nitrogen, a great variety of gaseous boron precursors has been used for experiments, but the most common ones are B_2H_6 and BCl_3, the former being advantageously used for low-temperature deposition in relation to its very low chemical stability, while the less dangerous latter has been used at higher temperatures. However, BF_3 is sometimes preferred to BCl_3 for chemical vapour infiltration (CVI) [8–10]. On the other hand, in spite of the high chemical inertness of dense BN, the CVD–BN deposits are sometimes attacked by moisture at room temperature [3, 11, 12].

In other respects, it has been pointed out that ceramic matrix composites (CMC) with no catastrophic failure could be obtained when a weak fibre–matrix bonding subsisted after composite processing [13–15]. In this case, the material failure results from several contributions: (i) crack propagation in the matrix via mode I, (ii) crack deviation at the fibre–matrix interface, (iii) crack propagation at this interface via mode II, (iv) load transfer from the matrix towards the fibres, (v) failure of fibres, and (vi) pull-out of fibres. Phenomena (ii), (iii), (iv) and (vi) which do not exist in brittle failure, increase the failure energy greatly, resulting in both high toughness and strength. This weak fibre–matrix bonding could be the result of the densification process itself (formation of a carbon layer) [16] or of the deposition of a fibre coating before densification [17–19]. In this way, the toughness reliability increases [19] and carbon can be advantageously replaced by boron nitride, which is more effective under oxidizing atmospheres [10, 18, 20–23]. In every case, the interphase has two actions: (i) it is a diffusion barrier which prevents the reaction between fibre and matrix and does not allow strong bonding between fibre and matrix [10]; (ii) it deviates the cracks from mode I to II; this point is probably

0022–2461

related, on the one hand to the anisotropic structure of both hexagonal BN and graphite (in the case of the hexagonal BN, the bonding energy between layers is reported to be 17 kJ mol^{-1} while the boron to nitrogen bond strength is reported as 635 kJ mol^{-1} [8]), and on the other hand to the interfacial stresses generated by the difference of the thermal expansion coefficient between the different phases, during cooling after matrix infiltration [10].

In a previous study, we developed CVI conditions to obtain BN deposits on fibres whose thickness was uniform over large fibre preforms ($150 \times 18 \times 10$ mm^3) [24]; here, we characterize, from a physico-chemical point of view, the BN films: firstly, as-deposited (i.e. deposited and post-treated under standard conditions), and secondly, taking into account the moisture action at room temperature. The analyses of the BN films were performed by X-ray photoelectron spectroscopy (XPS), micro-Raman spectroscopy (MRS), infrared spectroscopy (IRS), X-ray diffraction (XRD) and scanning electron microscopy (SEM).

2. Experimental procedure

2.1. Preparation of the BN films

As mentioned in a previous paper [24], the BCl_3–NH_3–H_2 mixtures have been preferred to BF_3–NH_3–H_2 ones to prevent the formation of the corrosive HF gaseous by-product. However, with BCl_3, the higher reactivity of this mixture produces various deposits, at any temperatures, whose chemical composition is a function of the temperature; then, pure BN is only obtained at sufficiently high temperature. Thus, our CVI reactor was designed to prevent the consumption of the inlet gas upstream of the deposition zone, although the formation of a small part of intermediate solids could not be completely avoided [24]. In spite of this problem, BN films were produced under a large range of deposition conditions (Table I); an important result of the CVI study with the BCl_3–NH_3–H_2 system is that, to obtain optimal BN thickness uniformity inside the whole fibre preforms, the deposition temperature must be decreased to 773 K.

The analyses have been performed on three kinds of samples, i.e. on carbon fibre preforms and on graphite bulk substrates, as previously reported [24], and on single silicon wafers placed on the top of the fibrous preform holder. This third substrate was used because in most of the analyses, the great similarity between carbon and boron nitride was a drastic drawback for the BN films characterization.

2.2. The characterization techniques

The chemical analyses of the deposits were performed by XPS with two spectrometers: the BN films deposited on carbon substrates (fibrous preforms or bulk rings) were investigated using an XPS AEI ES 200 B spectrometer (MgK_α, 12 kV, 20 mA) under a residual pressure of 10^{-6} Pa, labelled XPS spectrometer 1, while those on silicon wafers were investigated using a VG ESCALAB MK II spectrometer (MgK_α, 10 kV, 20 mA) under a residual pressure of $5\ 10^{-8}$ Pa, labelled XPS spectrometer 2. The C_{1s} core level of the hydrocarbon at 284.6 eV was used as an energy calibration. As a first step, the XPS spectra were decomposed by computer calculation, i.e. the lineshapes of individual peaks were fitted to gaussian spectral line functions. With both spectrometers, a non-linear background was subtracted and the fitting used a non-linear least square fitting method. In every case, the binding energies are quoted to $\pm$ 0.2 eV and the area ratio of the individual peaks (denoted in the text in X–Y terms) to $\pm$ 6%. Secondly, the atomic ratios were calculated from the XPS cross-section coefficients and the ratio between the total area of the XPS peak of two elements (denoted in the text in X/Y terms). The analyses were always carried out without any surface argon etching because it was reported that nitrogen sputtering was greater than that of boron [11]; these analyses are thus only representative of the external BN surface.

The BN deposits were also studied by IR and Raman spectroscopy; in these cases, silicon wafers were used as substrates. The IRS characterization was carried out with a BRUKER IFS 113-C spectrometer in reflection mode in the range 100–4500 cm^{-1} while the Raman characterization was carried out in back-scattering configuration using an argon incident laser beam and a JOBIN YVON double monochromator spectrometer in the range 20–3800 cm^{-1}. In comparison with IRS, this Raman apparatus has the advantage of allowing a local analysis (analysed area of about 1 μm^2 compared with 1 cm^2 for IRS).

The morphology of the BN films was examined by SEM (CAMBRIDGE Stereoscan 100) and the crystalline structure was determined by XRD (Philipps PW) on BN films deposited on silicon wafers.

TABLE I Preparation conditions for CVI–BN films

Deposition parameters	Deposition range	Standard deposition	Standard post-treatment
Temperature, T (K)	673–1173	773	1273
Total pressure, P (kPa)	0.13–13.3	0.27	Vacuum
Total flow rate, f (kg s^{-1})	10^{-6}–21×10^{-6}	3.5×10^{-6}	0
Volume flow rate ratios:			
NH_3/BCl_3	0–30	3	0
H_2/BCl_3	0–100	10	0
Time, t (h)	2–5	5	2

In addition to the analysis of the CVI-BN films, a reference sample of hexagonal BN (Cerac Pure Certified Chemicals) was examined using all the previous techniques.

3. Results

The first BN deposition experiments showed that the deposits were not stable in air at room temperature; i.e. when they were exposed to air, the coated samples produced a strong smell of ammonia and their mass increased with time. Consequently, the BN deposition step was followed by a standard post-treatment without any exposure to air (Table I) to reduce strongly the moisture effect; it consisted in heating the coated substrates at 1273 K for 2 h under a primary dynamic vacuum (nearly 5 Pa). Thus, generally, the BN films were prepared under standard conditions which consisted of one standard deposition and one standard post-treatment (Table I). Further studies of this moisture effect will be presented in Section 3.2.

3.1. Analyses of the BN films prepared under standard conditions

In this section, the exposure time in air was not controlled, but it was of the order of 1 month.

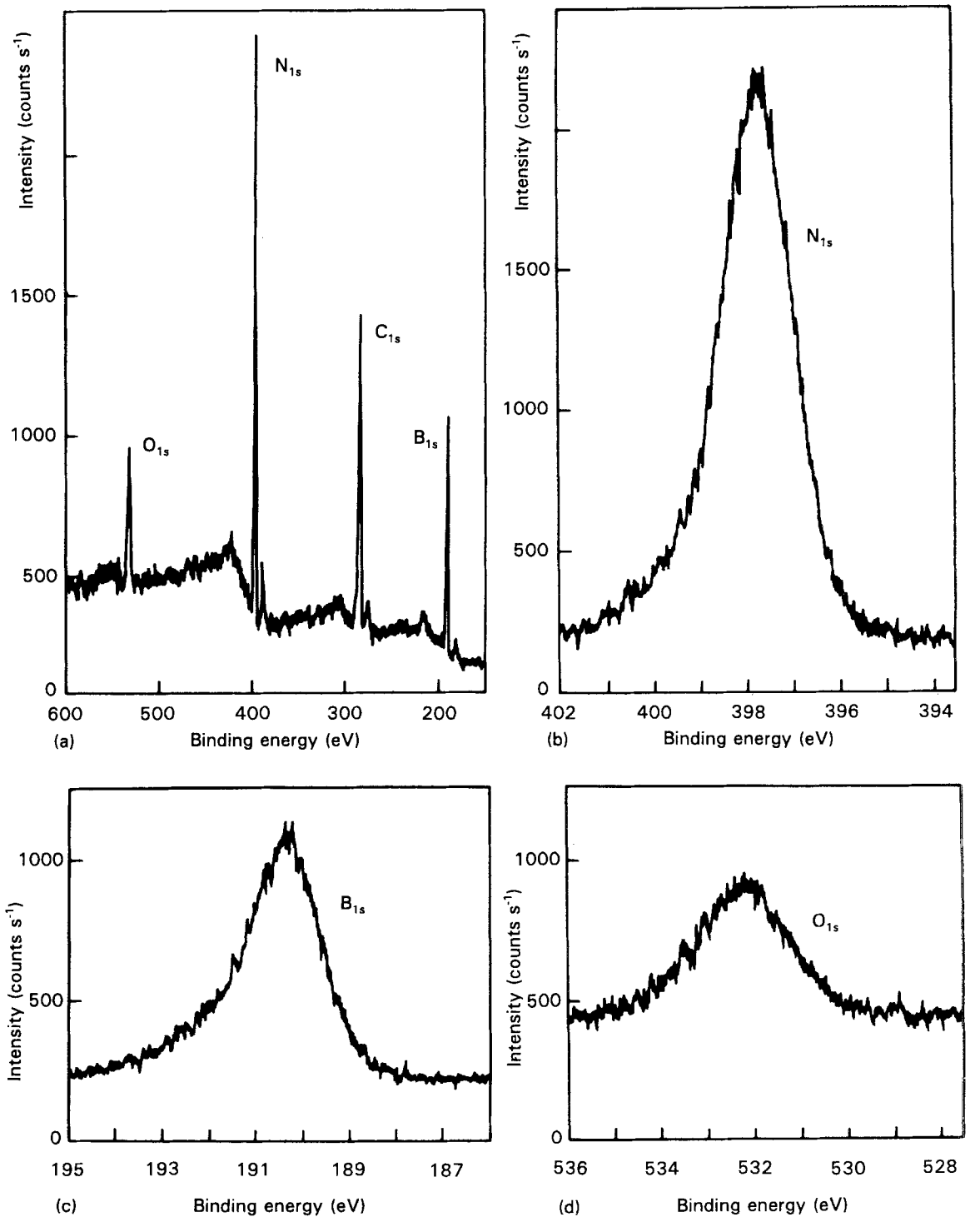

Figure 1 (a–d) Typical XPS spectra recorded from the BN films deposited on a fibrous preform with XPS spectrometer 1.

3.1.1. XPS qualitative analysis

Fig. 1 shows a typical XPS record obtained from the external surface of a BN film deposited on part of a fibrous preform by the XPS spectrometer 1. It reveals that the films contain boron, nitrogen, oxygen and carbon, but no chlorine. The carbon is frequently recorded in XPS and is attributed, in our case, to the surface contamination as classically made in XPS spectroscopy; but the detection of oxygen with such a high intensity, is unexpected (the gaseous precursors do not contain any oxygen), although some authors detected it in BN deposits synthesized by similar processes [10, 11, 25, 26]. An accurate resolution of the B_{1s} and N_{1s} spectra shows that each one results from several chemical bonds identified with the aid of the XPS Handbook [27] (Table II). Boron clearly appears to be linked to nitrogen with a binding energy (190.5 eV) corresponding to BN, but boron is also linked to oxygen in another part with a binding energy (of 192.6 eV). Nitrogen is, of course, linked to boron for the most important part, with a binding energy (397.6 eV) corresponding to BN, but its spectrum also shows a weak contribution of an unidentified elemental peak at 399.4 eV corresponding to a lower atomic charge. The width of the O_{1s} peak is rather larger than the others, but it is a classical situation in XPS spectroscopy, and moreover its binding energy is consistent with the data of Lacrambe [11]; thus no systematic decomposition was performed.

3.1.2. Influence of the CVI deposition parameters

First, to investigate the BN composition uniformity inside a same substrate loading, several elemental samples coated with BN in the same experiment were analysed (bulk or fibrous, in superior or inferior position in the deposition zone, in internal or external position in the preform). Table III shows that although there are some variations from one place to another, the composition of the BN films appears nearly uniform: about 20% of boron atoms is linked with oxygen atoms, and the other boron atoms are linked with nitrogen atoms. Table III also reports the composition of the hexagonal BN reference analysed by the XPS spectrometer 1.

The variations of the chemical composition of the BN films were investigated as functions of the CVI deposition parameters varying over all the range defined in Table I. From all these analyses, three classes can be distinguished which are reported in Table IV: (i) most XPS analyses lead to B–N values in the range 70%–90% (and accordingly B–O values in the range 10%–30%), the calculation of the average composition, composition A, leads to values very close to the average analysis reported in Table III; (ii) two XPS analyses lead to a composition richer in nitrogen and poorer in oxygen (B–O is lower than 10%); they are obtained on films deposited at high temperature (1073 and 1173 K) whose average analysis is composition B; (iii) five XPS analyses show that deposits carried out at very low total flow rates (1×10^{-6} or 2×10^{-6} kg s^{-1}) or with a BCl_3 excess ($NH_3/BCl_3 = 1/3$) have a very strong non-stoichiometry (B–O is higher than 30%) whose average analysis is composition C.

From all the results, some general rules can be distinguished: B–N and N/B are generally very close, O/B is always greater than B–O, oxygen and nitrogen contents vary in opposite ways, (O + N)/B is always slightly greater than 1 and tends to increase with the oxygen content.

Table V shows the XPS analyses of the five XPS analyses reporting B–O values greater than 30%, taking into account the computing decomposition of the N_{1s} peak. For each one, the appearance of a

TABLE II Nature and binding energies of the chemical bonds detected by XPS analysis from XPS spectrometer 1

B_{1s}		N_{1s}		O_{1s}
B–N	B–O	N–B	N–?	O–?
190.5 eV	192.6 eV	397.6 eV	399.4 eV	531.9 eV

TABLE IV Average chemical composition of BN films of the three categories A, B and C (all values are presented as percentages)

	A	B	C
O/B	35	20	51
N/B	81	86	69
(O + N)/B	116	106	120
B–O	19	08	34
B–N	81	92	66

TABLE III Variations of the chemical composition measured by XPS as a function of the sample position in the deposition zone for a BN film prepared under standard CVI conditions

Place	Sup bul	Inf bul	Sup ext	Inf ext	Sup int	Inf int	Average	BN ref
O/B	29	31	39	38	33	33	34	06
N/B	82	83	85	78	78	83	81	90
(O + N)/B	111	114	124	116	111	116	115	96
B–O	21	21	18	22	17	13	19	0
B–N	79	79	82	78	83	87	81	100

Notes: Sup bul, superior bulk graphite ring; inf bul, inferior bulk graphite ring; sup ext, superior external fibrous elemental part; inf ext, inferior external fibrous elemental part; sup int, superior internal fibrous elemental part; inf int, inferior internal fibrous elemental part (all values are presented as percentages). BN ref, the results obtained with the hexagonal BN powder from Cerac Pure Certified Chemicals.

TABLE V Decomposition of the five XPS N_{1s} peaks obtained from the BN films classified in the category C in Table IV (all values are presented as percentages)

	NH_3/BCl_3 = 1/3	1×10^{-6} kg/s– 266 Pa	2×10^{-6} kg/s– 266 Pa	1×10^{-6} kg/s– 1.33 kPa	2×10^{-6} kg/s– 1.33 kPa	Average
O/B	64	47	39	61	45	51
N/B	61	71	79	64	72	70
(O + N)/B	125	118	118	125	117	121
B–O	36	34	32	36	32	34
B–N	64	66	68	64	68	66
N–B	77	65	85	83	84	79
N–?	23	35	15	17	16	21

second nitrogen contribution at a binding energy of 399.4 eV is evident and the N–? values which are, on average, 21%, are very much higher than those noted in the other cases which stay in the range 5%–7%.

3.1.3. Other characterizations

Fig. 2a shows the XRD pattern of a CVI-BN film (1.4 μm) deposited on a silicon wafer and, for comparison, the hexagonal BN reference pattern is reported in Fig. 2b. The CVI-BN film only exhibits a very broad halo, corresponding to the space between the BN layers, centred at a distance $d = 0.36$ nm greater than for BN reference ($d_{0\,0\,2} = 0.333$ nm). From the Scherrer relation [28] and the measurement of the half-width of the broad halo, the size of the BN crystallites is nearly 1.5 nm. On the other hand, no (1 0) diffraction, corresponding to the cumulation of the broad X-rays reflection on both (1 0 0) and (1 0 1) planes, was observed and it was verified that CVI-BN films whose thickness is lower than 1 μm never produced any X-ray diffraction peak.

Fig. 3a shows the variations of the reflection coefficient of the BN films measured by IRS. The two typical vibration modes of the hexagonal BN appear with low intensities: at 1390 cm^{-1} corresponding to the B–N stretching, and at 790 cm^{-1} corresponding to the B–N–B bending. Fig. 3b shows the variations of the reflection coefficient of the same BN films measured after a 60 days ageing at room temperature and under an air atmosphere. The same vibrational modes subsist, but they have lower intensities and a broad peak appears at nearly 1500 cm^{-1}. A similar absorption has been reported by Lacrambe and Dugne who attributed it to the formation of B–O bonds [10, 11].

MicroRaman spectroscopy of the CVI-BN films shows a vibrational mode at about 1375 cm^{-1} (due to boron and nitrogen atoms moving against each other)

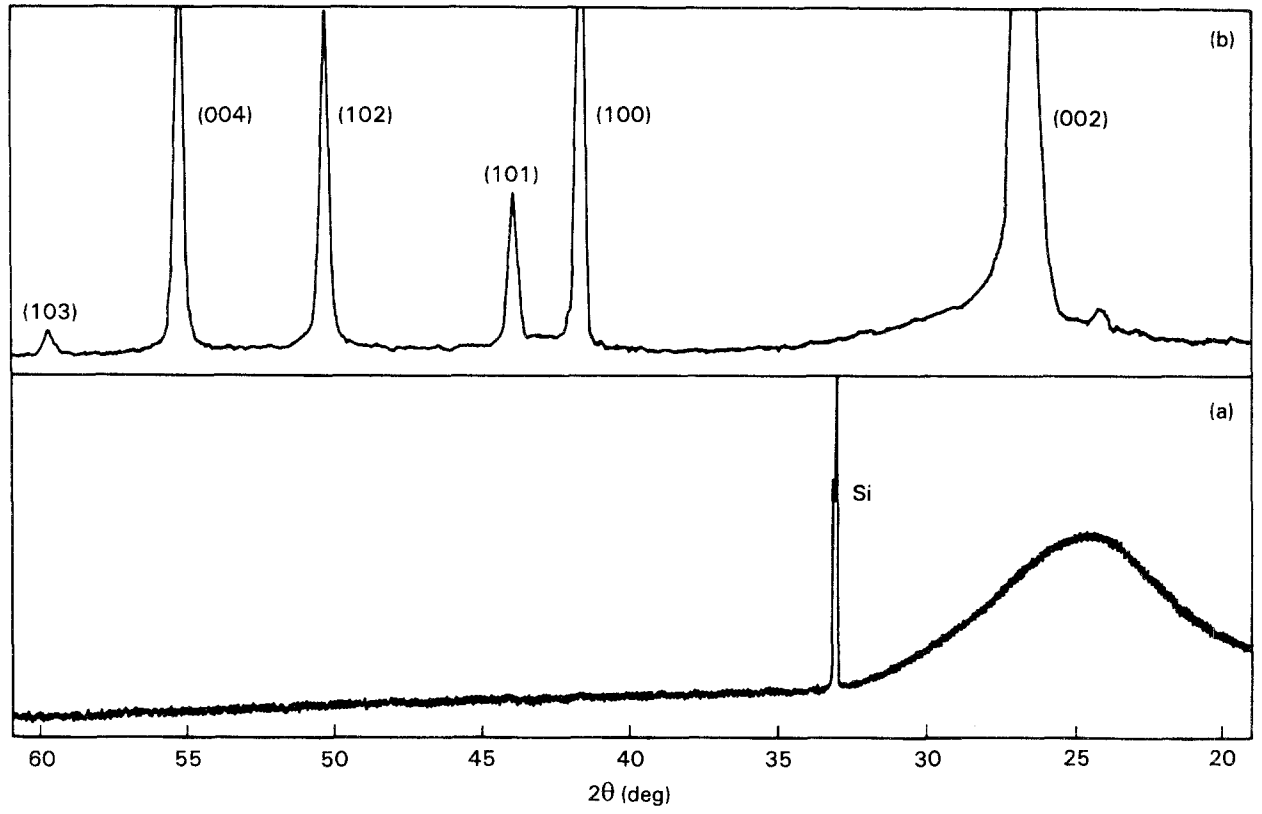

Figure 2 XRD patterns of BN: (a) BN film deposited on a silicon wafer (BN thickness 1.4 μm), (b) BN reference.

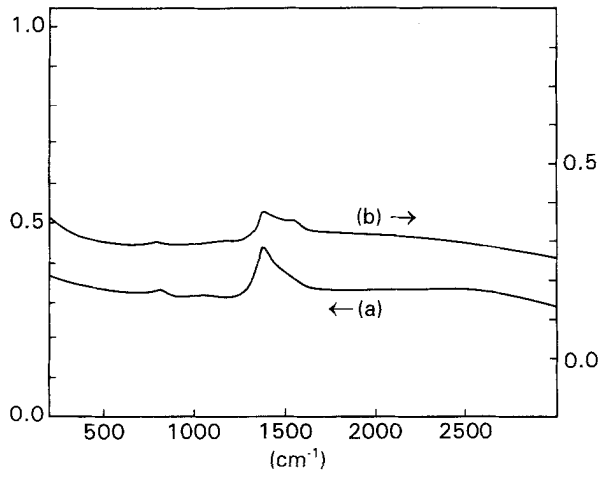

Figure 3 IR spectra showing the variations of the reflection coefficient of the BN films deposited on a silicon wafer: (a) without air exposure, (b) with an air exposure time of 60 days.

which increases with the BN thickness (Fig. 4a–c) and which is slightly shifted towards high wave numbers in comparison with hexagonal BN reference (1365 cm^{-1}) (Fig. 4d); this behaviour is consistent with the study of Nemanich who reported that this high-frequency, E_{2g}, mode of BN increased when the crystallite size decreases [29]. The second active Raman mode of BN at 52 cm^{-1}, due to the whole planes sliding against each other, is not observed.

From a morphological point of view, the CVI-BN films are transparent and produce optical reflection fringes. When they are deposited on carbon fibres of a three-dimensional preform, they constitute a regular layer (Fig. 5). The measurements of both the mass and the thickness of BN allow estimation of the deposit density, which is about 1.4 $g\,cm^{-3}$ when the deposition is carried out at 773 K [24]. This rather low density, in comparison with the theoretical density

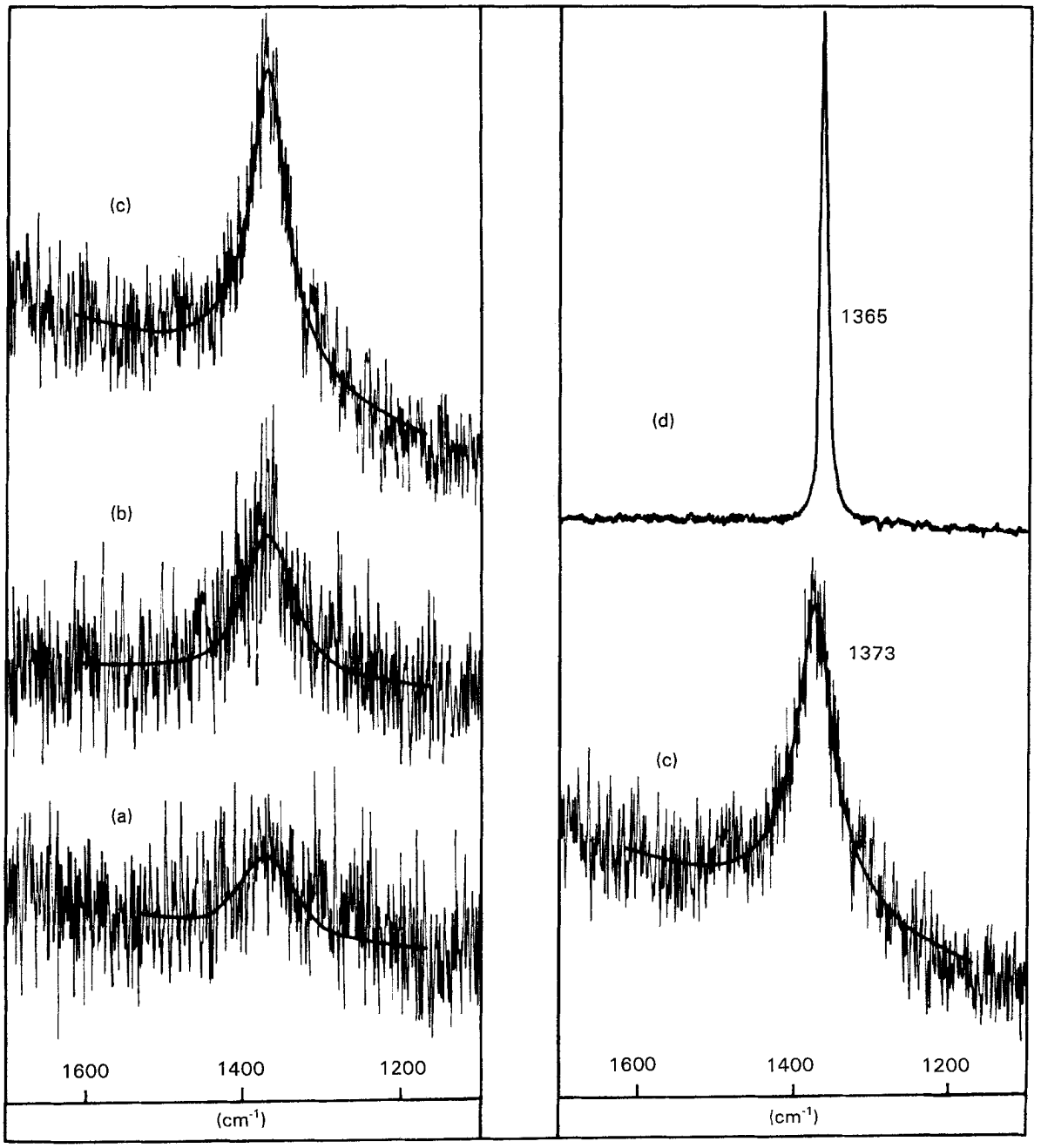

Figure 4 Micro-Raman spectra of the BN films deposited on silicon wafers as function of the film thickness: (a) 0.3 μm, (b) 0.75 μm, (c) 1.4 μm, (d) BN reference.

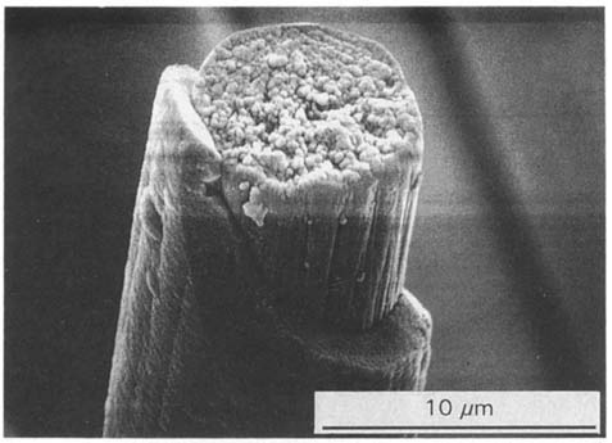

Figure 5 Morphology of the BN layer deposited on the fibres of the fibrous preform.

($2.27\,g\,cm^{-3}$) is in good agreement with previous works [8, 10, 11, 30].

3.2. The effect of moisture on the BN films

3.2.1. Preliminary study

A short study of the BN mass variation was carried out before the CVI study to limit the action of moisture.

Fig. 6 reports the average relative mass variations of the BN films deposited on the 30 elemental parts of a fibrous carbon preform, as a function of air exposure time (limited to 48 h) for deposition temperatures in the range 773–1273 K and with or without the standard post treatment (Table I). It appears that (i) the variations of the BN mass increase when the deposition temperature decreases, (ii) the post-treatment reduces this variation, but cannot remove it, (iii) the mass variations are identical over all the 30 elemental substrates, (iv) the mass variations are similar to those reported by Lacrambe [11].

The post-treatment was limited to 1273 K to develop a BN film process compatible with the BN deposition on Nicalon fibres whose mechanical properties decrease when they are subjected to higher temperatures. The dynamic vacuum allows a pressure increase to be noted at the beginning of the post-treatment. Otherwise, when the BN films were exposed to air, the ammonia smell became very weak.

On the other hand, after an air exposure time of 150 h, a second standard post-treatment was carried out to simulate the heating at the beginning of the CVI densification of the preforms. Table VI shows that the BN mass, measured immediately after cooling, decreases, but an effective BN mass increase of nearly 5% was not removed, in comparison with the initial BN mass; after a second air exposure for an identical time, the mass variation returns to the previous level.

3.2.2. Growth of the "destabilization crystals"

The examination of the BN films after a very long air exposure time reveals white crystals. Fig. 7a shows one of these growing crystals on a silicon wafer after 60 days in air while Fig. 7b shows one growing on a carbon fibre after 150 days in air; in the latter case, its appearance can be bulk (Fig. 7b) or foliated (Fig. 7c). Around these crystals, the variation of the coloured

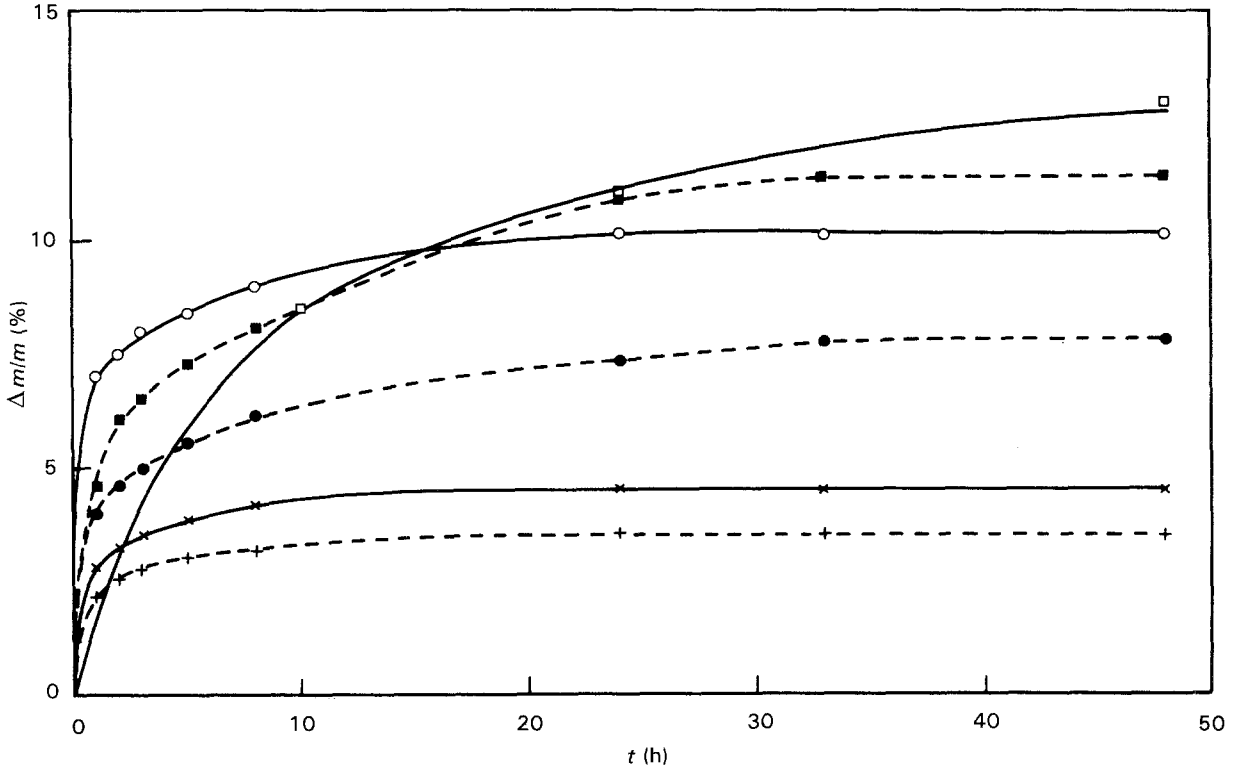

Figure 6 Relative mass variations of the BN films deposited on the fibrous preforms as a function of air exposure time for different deposition temperatures and with (+ PT) or without (− PT) the standard post-treatment (Table I). (×) 1273 K − PT, (+) 1273 K + PT, (○) 873 K − PT, (●) 873 K + PT, (■) 773 K + PT, (□) 1273 K + PT at 1573 K [11].

TABLE VI Variations of BN mass with respect to the initial BN (without air exposure) as a function of successive ageing conditions (air exposure, heating at 1273 K, air exposure)

	1st air exp. (150 h)	Heating at 1273 K–2 h	2nd air exp. (150 h)
BN mass variation (%)	11	5	11

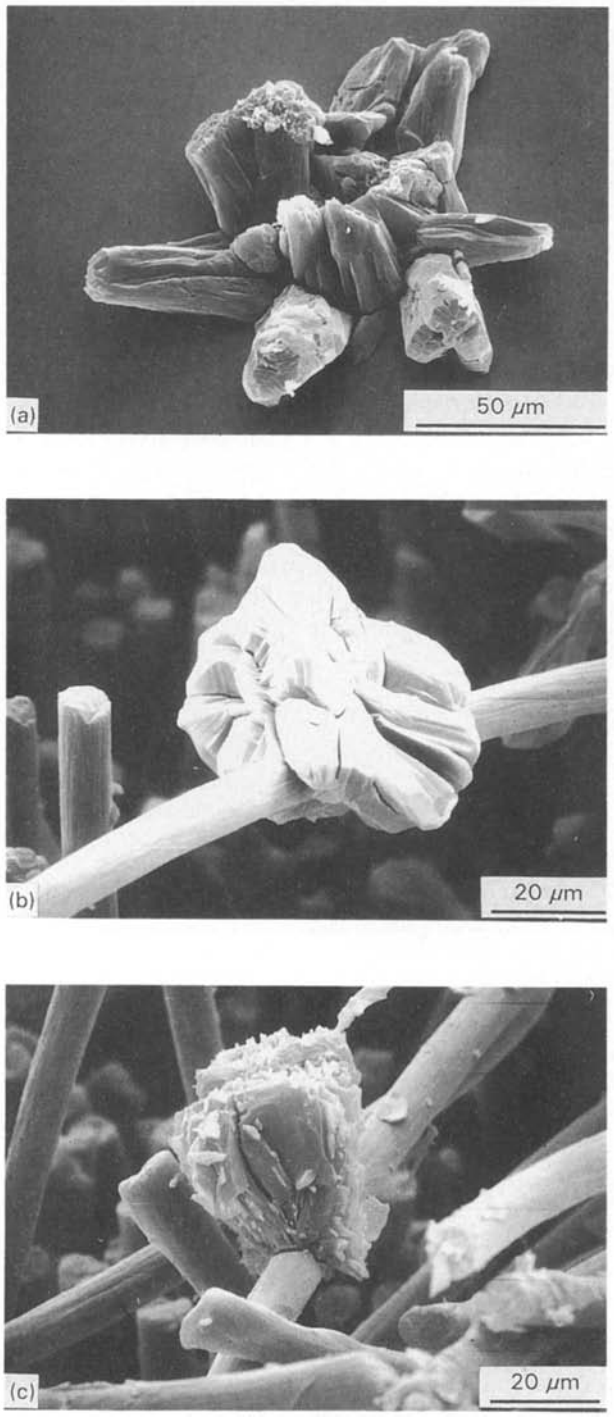

Figure 7 (a) A "destabilization crystal" growing on a silicon wafer after 60 days at air, (b) another crystal growing on a carbon fibre after 150 days at air showing a bulk appearance, (c) a crystal growing on a carbon fibre after 150 days in air showing a foliated appearance.

fringes indicates that the BN is consumed by the crystal growth. A similar crystal growth was reported by Rand and Roberts [3] who identify them by electron diffraction as single-crystal boric acid, and by Matsuda [12] who identified them as the ammonium borate hydrate $(NH_4)_2O \cdot 5B_2O_3 \cdot 8H_2O$ by IR spectroscopy of BN powder.

These crystals were examined by MRS to determine the nature of the crystals, after verifying by EDAX that they do not contain any element heavier than neon. MRS was preferred to IRS because it allows a local analysis. Fig. 8 shows four Raman spectra, recorded in the range 0–3800 cm^{-1} on (a) a "destabilization crystal", (b) di-boron trioxide (Merck), (c) boric acid powder (Aldrich Chemical Company, Inc), (d) ammonium tetraborate tetrahydrate $(NH_4)_2O \cdot 2B_2O_3 \cdot 4H_2O$ (Aldrich Chemical Company, Inc); unfortunately the ammonium borate hydrate identified by Matsuda could not be found. It clearly appears that the destabilization does not produce pure B_2O_3, spectra (c) and (d) present some similarities with spectrum (a), but no complete identification is achieved.

3.2.3. Influence of different post-treatments

3.2.3.1. Preparation of the samples. Besides the CVI study, some specific experiments were carried out to study the influence of six different post-treatments on the ageing of the BN films deposited under standard CVI conditions. These post-treatments were

(I) without any post-treatment,
(II) standard post-treatment (1273 K, vacuum, 2 h),
(III) post-treatment under nitrogen (1273 K, 1.33 kPa, 10^3 cm^3 min^{-1}, 2 h),
(IV) post-treatment under hydrogen (1273 K, 1.33 kPa, 10^3 cm^3 min^{-1}, 2 h),
(V) post-treatment under ammonia (1273 K, 1.33 kPa, 10^3 cm^3 min^{-1}, 2 h),
(VI) high-temperature post-treatment (1473 K, vacuum, 2 h).

The BN films were deposited simultaneously on fibrous preforms and on silicon wafers. The mass variations of the fibrous preforms coated with BN were recorded over 1 month (they were not cut in 30 elemental parts, but prepared in monolithic form to increase the accuracy of the mass variations); this ageing consisted in a succession of five steps:

(1) a first air exposure at room temperature for 17 days,
(2) drying at 373 K under an air atmosphere for 84 h where the adsorbed water is evaporated,
(3) a second air exposure at room temperature for 9 days,
(4) heating at 1273 K under dynamic vacuum for 2 h,
(5) a third air exposure time at room temperature for 3 days.

On the other hand, the BN films deposited on silicon wafers were exposed to air for selected times (0, 3, 30, 300 h) and then set inside a desiccator under

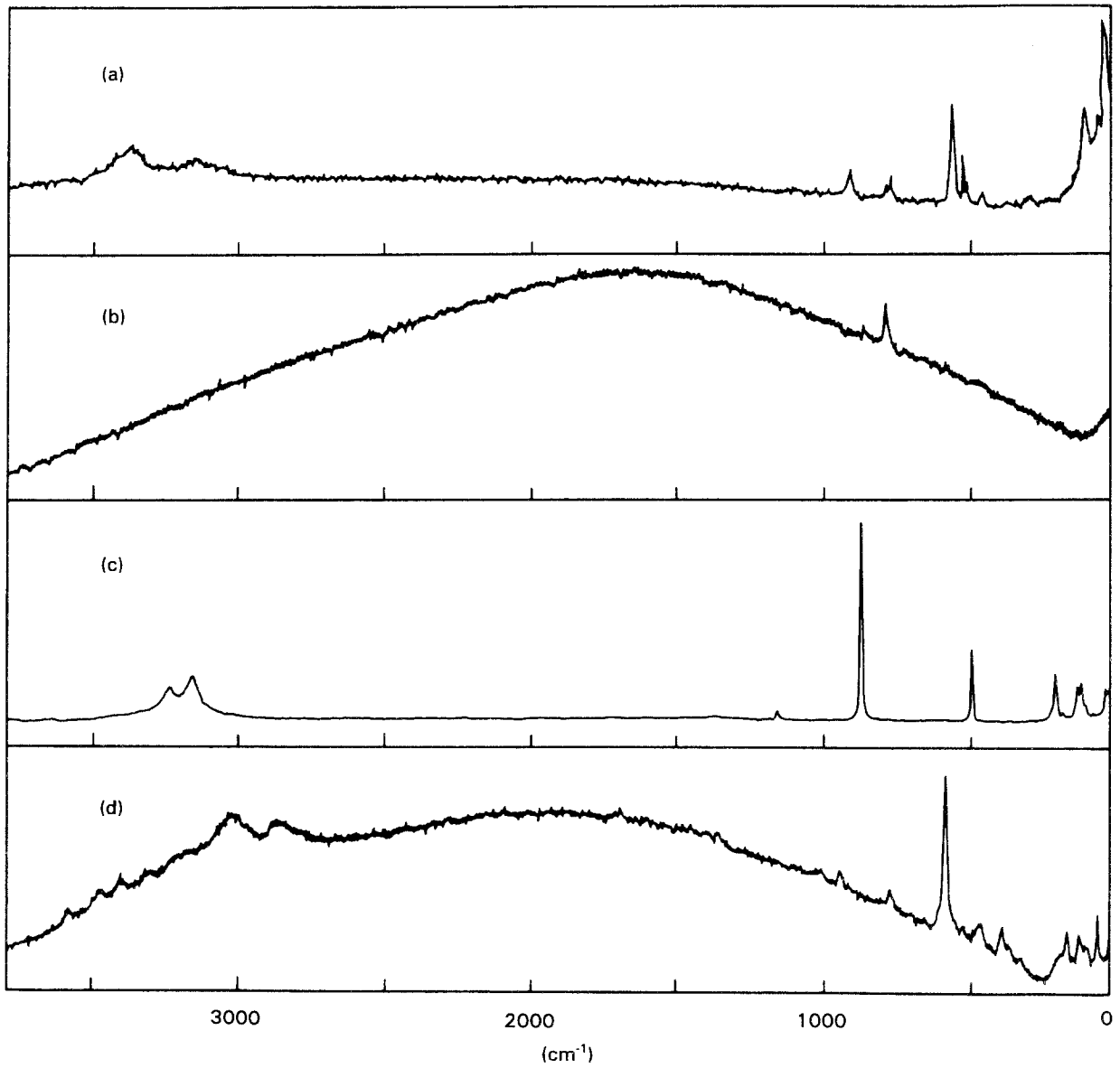

Figure 8 Micro-Raman spectra: (a) a "destabilization crystal", (b) di-boron trioxide, (c) boric acid powder, (d) ammonium tetraborate tetrahydrate $(NH_4)_2O \cdot 2B_2O_3 \cdot 4H_2O$.

vacuum to stop moisture action until they were analysed with the XPS spectrometer 2.

3.2.3.2. BN mass variations. Fig. 9 shows the mass variations of BN deposited on the fibrous preforms as functions of the ageing conditions, and, to simplify the presentation, the relative BN mass variations during each ageing step are reported in the Table VII, for the six post-treatments. The column "(2)/(1)" reports the relative BN mass variation during the first air exposure at room temperature. The column "1 + 2 + 3 + 4" reports the algebraic sum of the BN mass variations occurring in the ageing steps (1), (2), (3) and (4), and thus, it allows comparison of the BN mass after the second post-treatment at 1273 K with the initial BN mass.

Firstly, some general comments, valid for the six post-treatments, can be made. (i) At the beginning of the air exposure (for almost 6 h), the BN mass increases strongly, as seen in Fig. 6; (ii) at greater air exposure time, the BN mass variations are correlated with the relative humidity, reported at the bottom of Fig. 9; (iii) one part of the BN mass increase corresponds to an adsorption of water which can be evaporated by drying (column "(2)/(1)" in Table VII); (iv) after heating at 1273 K (4), the resulting BN mass becomes lower than the initial BN mass, indicating a consumption of one part of the BN films; such a result is contrary to the previous result reported in Table VI, where the air exposure time was shorter.

On the other hand, there is a large difference between the post-treated BN-coated preforms (II–VI) and the unstabilized BN-coated preform (I) in terms of BN mass variations, as reported in Table VII. Without any post-treatment, the BN mass increases by 66% in step (1), and loses only 42% of this mass increase (column "(2)/(1)") during drying (2), and finally, the BN mass decreases by 72% during heating (4). In the other cases and on average, the BN mass increases by 24%

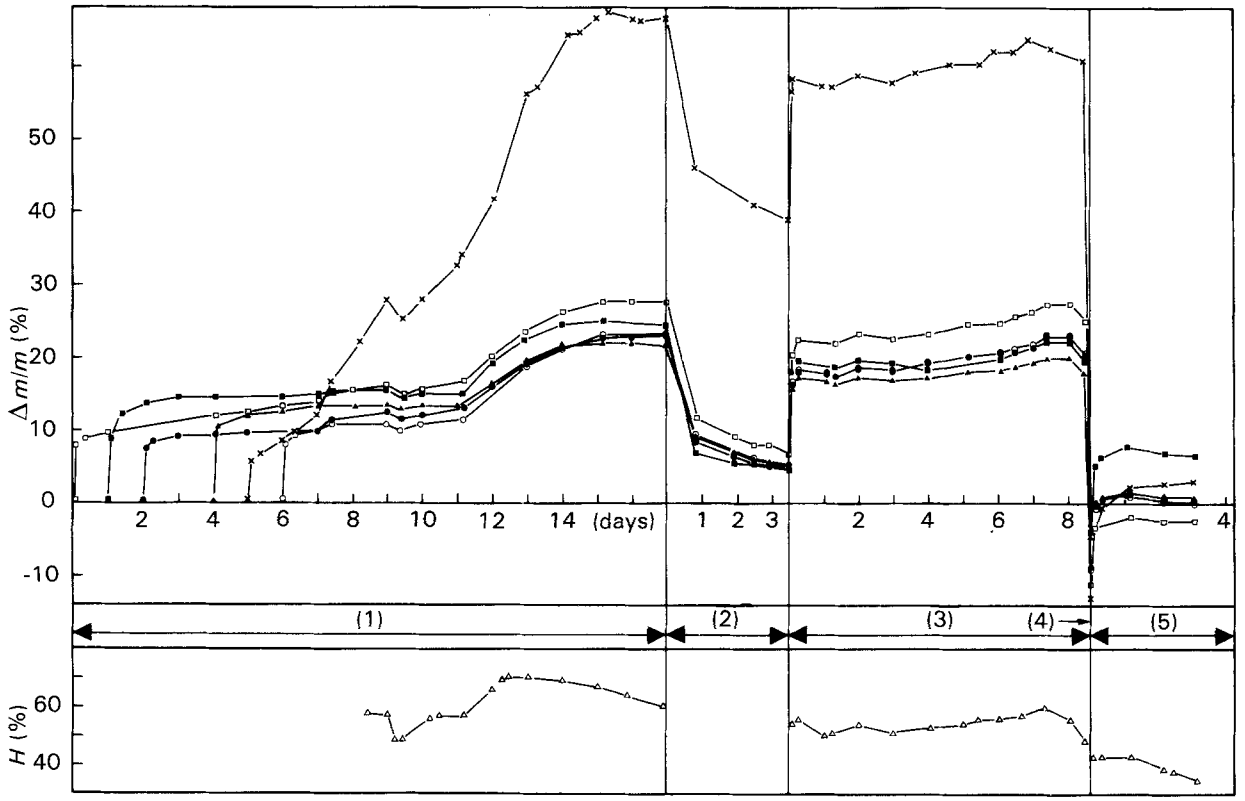

Figure 9 Relative mass variations of the BN films deposited on the fibrous preforms as functions of the ageing conditions for the six post-treatments (the variations of the relative humidity, H (%) are reported at the bottom of the figure). (×) (I) with no post-treatment, (○) (II) standard post-treatment (1273 K, vacuum, 2 h); (●) (III) post-treatment under nitrogen (1273 K, 1.33 kPa, 1000 $cm^3 min^{-1}$, 2 h); (□) (IV) post-treatment under hydrogen (1273 K, 1.33 kPa, 1000 $cm^3 min^{-1}$, 2 h); (■) (V) post-treatment under ammonia (1273 K, 1.33 kPa, 1000 $cm^3 min^{-1}$, 2 h); (▲) (VI) high-temperature post-treatment (1473 K, vacuum, 2 h).

TABLE VII The relative variations of the BN mass during the different ageing steps (1–6) defined in text, for the six post-treatments also defined in text

	BN mass (%)						
Post-treat.	(1)	(2)	(2)/(1)	(3)	(4)	1 + 2 + 3 + 4	(5)
(I)	+ 66	− 28	− 42	+ 22	− 72	− 12	+ 16
(II)	+ 23	− 18	− 78	+ 15	− 29	− 9	+ 9
(III)	+ 23	− 18	− 78	+ 15	− 29	− 9	+ 9
(IV)	+ 28	− 21	− 75	+ 18	− 36	− 11	+ 9
(V)	+ 24	− 20	− 80	+ 15	− 24	− 5	+ 11
(VI)	+ 22	− 17	− 77	+ 13	− 23	− 5	+ 6

in step (1), and loses 78% of this mass increase (column "(2)/(1)") during the drying (2) and finally, the BN mass decreases by 28% during heating (4) (Table VII).

Smaller differences also exist between the five post-treatments (II–VI). (i) The post-treatments under dynamic vacuum (II) or under nitrogen (III) have the same stabilization effect; (ii) the post-treatment under hydrogen (IV) leads to a slightly less efficient stabilization in comparison with the standard stabilization (II) (at air exposure, the BN mass increases are greater, the fraction of the adsorbed water is lower, the heating produces a greater BN mass decrease, which finally leads to a greater consumption of deposit (column "1 + 2 + 3 + 4"); (iii) the post-treatment under ammonia (V) leads to a more efficient stabilization than the standard one (II) (a greater part of the initial mass increase corresponds to adsorbed water and the heating produces a lower BN mass decrease, which results in a lower consumption of deposit (column "1 + 2 + 3 + 4"); (iv) the post-treatment under dynamic vacuum at high temperature (VI) leads to a stabilization very similar with the post-treatment under ammonia (V) (the BN mass variations are weaker but they result in an identical consumption of deposit (column "1 + 2 + 3 + 4").

3.2.3.3. XPS analysis. (a) The aged BN-coated preforms. After ageing, the fibrous preforms were analysed by the XPS spectrometer 1 (Table VIII) to compare their composition with the average composition (A) presented in Table IV; this comparison allows

TABLE VIII Influence of the post-treatments (I)–(VI) defined in the text on the chemical composition of the BN films deposited on monolithic fibrous preforms after ageing (all values are presented as percentages)

	(I)	(II)	(III)	(IV)	(V)	(VI)	(A)
O/B	83	50	34	46	35	27	35
N/B	60	68	77	74	81	81	81
O + N/B	143	118	111	120	116	108	116
B–O	39	28	24	20	14	17	19
B–N	61	72	76	80	86	83	81
N–B	88	93	95	95	95	95	94
N–?	12	7	5	5	5	5	6

the effects of both the different post-treatments and the subsequent ageing to be seen compared with the standard BN preparation.

Accordingly with its high BN mass variation, the ageing of unstabilized BN film (I) produces a very strong composition change: B–O increases up to 39% while the second contribution of the nitrogen peak increases up to 12%. The analyses reported in columns II and A correspond to BN films produced under the same conditions with the exception that the former was heated at 1273 K under dynamic vacuum for 2 h after an air exposure of 29 days; then, it appears that this second heating leads to an oxygen content increase (B–O increases from 19% to 28%). The other post-treatments can be classified as in Section 3.2.3.2. Actually, the post-treatment under nitrogen (III) produces a BN stabilization similar to that obtained by the post-treatment under vacuum (II); the post-treatment under hydrogen (IV) produces a stabilization slightly better (B–O decreases to 20%). On the other hand, the two post-treatments under ammonia (V) and at 1473 K (VI) lead, after ageing, to a weak increase of the BN stoichiometry (B–N increases up to 86% and 83% respectively).

(b) The BN/Si materials. Fig. 10 shows a typical XPS record obtained from the BN film deposited on a silicon wafer using the XPS spectrometer 2. Table IX gives the compositions, obtained by the XPS spectrometer 2, of the hexagonal BN reference and the BN films deposited on the silicon wafers, measured as functions of both the type of post-treatment and air exposure time. It must be noted that the exposure time in air of these BN/Si materials was controlled at values between 0 and 300 h, while the exposure time of the BN deposited on the fibrous preform was never controlled, but on average, it was between 1 and 2 months. The analyses of the same BN reference with the XPS spectrometers 1 and 2 (Tables III and IX) lead to slightly different results, but these quantitative differences are quite consistent with the accuracy of the XPS measurements.

When compared with Table II, Table X shows that the XPS spectrometers 1 and 2 lead to nearly the same binding energies of the chemical bonds, except for B–O. The XPS analyses of all the BN-coated silicon wafers give the B–O peak at 191.8 eV, except for one sample which gives it at 192.6 eV; this sample corresponds to the BN-coated silicon wafer which was not post-treated and exposed to air for 300 h; at the same time, the aged BN-coated preform produced under identical conditions, presents the highest BN mass variation in air (Section 3.2.3.2).

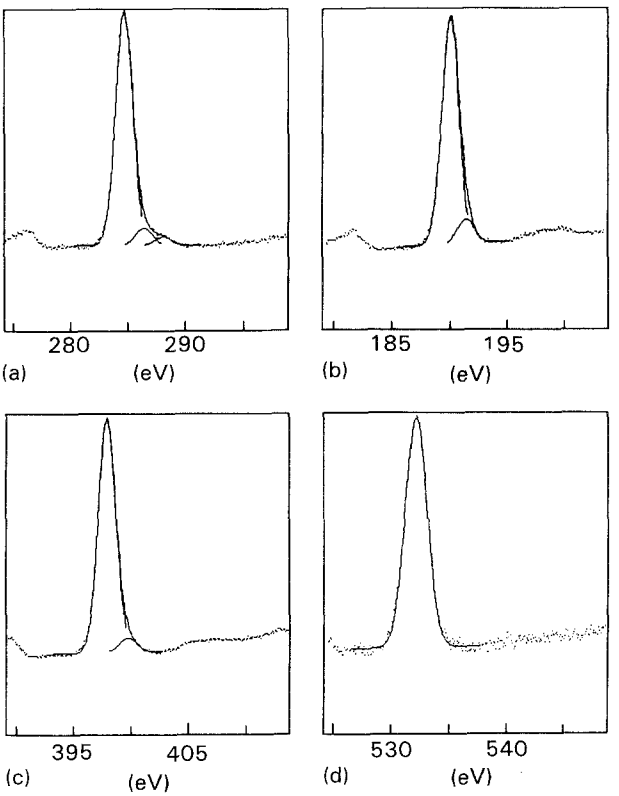

Figure 10 Typical XPS spectra recorded from the BN film deposited on a silicon wafer by XPS spectrometer 2. (a) C 1s, (b) B 1s, (c) N 1s, (d) O 1s.

The study of the surface contamination with carbon, using XPS spectrometer 2, shows that its peak can be decomposed into three parts, C(1), C(2), C(3), which correspond, respectively, to carbon linked with other carbon atoms (C–C), carbon linked with an hydroxyl group (C–OH), and carbon linked with an oxygen atom (C=O) (Fig. 10) as already mentioned [11]; otherwise, the different parts of this decomposition do not vary significantly and although the C/B ratios present some variations, they can be summarized as the following average values (Table IX): C(1) = 88, C(2) = 8, C(3) = 4 and C/B = 82 (or 96 in the case of the post-treatment (I)). On the other hand, the general rules, distinguished as B–O, B–N, O/B, N/B and (O + N)/B (Section 3.1.2) by XPS spectrometer 1, are still valuable for the BN/Si materials analysed by XPS spectrometer 2. With the help of the resolution of the C_{1s} spectrum, it appears possible to

TABLE IX Chemical compositions of the BN films deposited on the silicon wafers, measured by the XPS spectrometer 2, as functions of both the type of post-treatment (X) defined in the text and the air exposure time, t in hours (all values are presented as percentages)

(X)	t	C(1)	C(2)	C(3)	B–N	B–O	N–B	N–?	N/B	O/B	C/B	O + N/B
I	0	88	8	4	91	9	94	6	103	21	76	124
	3	86	9	5	89	11	93	7	100	27	93	127
	30	87	8	5	85	15	92	8	100	37	117	137
	300	86	11	3	75	25	93	7	90	56	100	146
II	0	90	8	2	89	11	94	6	96	20	57	116
	3	88	7	5	88	12	94	6	99	25	87	124
	30	88	8	4	89	11	94	6	98	27	86	125
	300	91	7	2	87	13	94	6	96	32	88	128
III	0	90	7	3	88	12	97	3	101	23	65	124
	3	87	9	4	88	12	95	5	97	27	78	124
	30	87	9	4	88	12	94	6	97	28	80	125
	300	81	16	3	86	14	94	6	97	30	89	127
IV	0	87	9	4	84	16	94	6	93	29	86	122
	3	89	8	3	85	15	95	5	94	31	87	125
	30	88	8	4	85	15	95	5	93	32	89	125
	300	88	9	3	84	16	97	3	93	34	68	127
V	0	88	9	3	92	8	95	5	99	19	82	118
	3	88	8	4	89	11	93	7	98	21	87	119
	30	88	8	4	89	11	94	6	100	24	96	124
	300	87	9	4	89	11	93	7	99	23	84	122
VI	0	90	7	3	90	10	94	6	98	19	86	117
	3	89	7	4	91	9	94	6	98	19	81	117
	30	88	7	5	90	10	94	6	98	21	84	119
	300	88	7	5	90	10	94	6	98	22	77	120
BN	ref	92	8	0	100	0	100	0	106	4	9	110

TABLE X Nature and binding energies of the chemical bonds detected by XPS analysis on XPS spectrometer 2

C_{1s}(eV)			B_{1s}(eV)		N_{1s}(eV)		O_{1s}(eV)
C(1)	C(2)	C(3)	B–N	B–O	N–B	N–?	O–?
284.6	286.2	288.0	190.2	191.8	397.8	399.6	532.2

correlate B–O and O/B taking into account both the stoichiometry change from BN to B_2O_3, which is the final compound of the oxidation of BN, and the part of oxygen linked to the carbon contamination. Similar to the XPS analyses performed on spectrometer 1, the resolution of the O_{1s} spectrum is not reliable, because all chemical bonds of oxygen (with boron, carbon or hydrogen) produce individual peaks in the same range, which leads to a larger spectrum compared to others (Fig. 10).

The amount of BN film destabilization appears only in the O/B and O + N/B terms for all the post-treatments and also in B–O (and B–N) terms for post-treatment (I), and Fig. 11 which represents the O/B variations for all the post-treatments as a function of time. The distinction between the different post-treatments, already mentioned in Sections 3.2.3.2 and 3.2.3.3, can be used again. With no post-treatment, O/B quickly increases, while with a post-treatment, O/B increases very slowly. Of the post-treatments, that under hydrogen (IV) leads to O/B values higher than those under dynamic vacuum (II) or under nitrogen (III), both the latter values being similar; on the other hand, post-treatments under ammonia (V) or under high temperature (VI), which appear similar, lead to the lowest O/B values. Otherwise, it seems that the post-treatments (II), (III) and (IV) produce BN films with an initial oxygen content (t = 0 h) higher than in the absence of post-treatment, while post-treatments (V) and (VI) lead to a low initial oxygen content in comparison with post-treatment (I).

3.2.3.4. Morphological examination. SEM examination of the BN/Si materials shows the formation of the "destabilization crystals" already reported in Section 3.2.2. Their density on the surface and their average size are particularly high after 300 h in air, especially in the case of post-treatment (I) (Fig. 12a and b) in comparison with the BN films prepared under the same conditions but not exposed to air (Fig. 12c and d; in this case, the air exposure is limited to some transfers between the desiccator, the CVI reactor and the characterization apparatus). In the case of the other post-treatments, some destabilization crystals can be seen, with a density and an average size which are similar to those of Fig. 12c and d. It seems that they do not change with the air- exposure time. (Please note that the magnifications are different in Fig. 12.)

SEM examination was also carried out on the aged BN-coated preforms. In the case of post-treatment (I), the carbon fibres appear to be extensively damaged, some being punched with large holes (Fig. 13a). After post-treatments (II), (III) and (IV), it seems that the

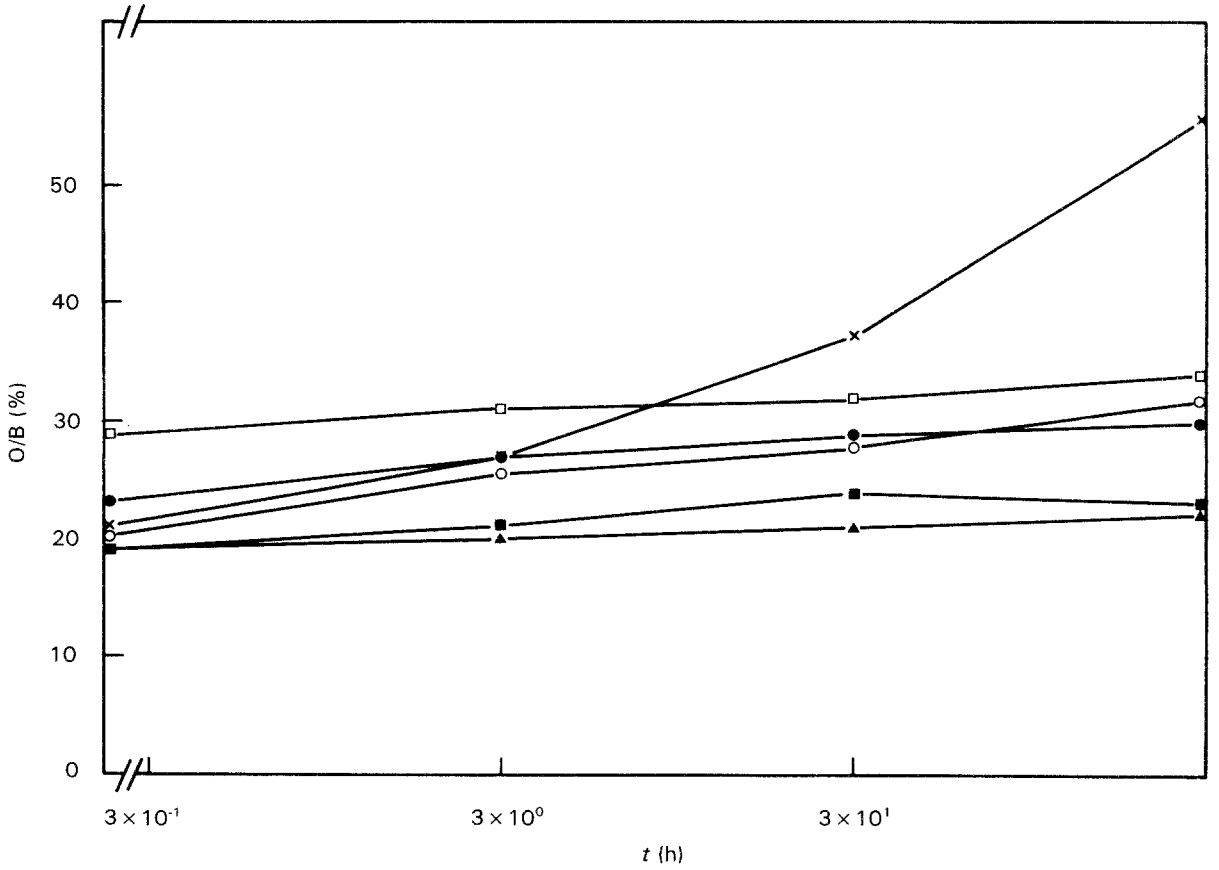

Figure 11 Variations of the O/B contents as a function of the exposure time in air, for the six post-treatments I–VI (XPS spectra were recorded on BN/Si materials by the XPS spectrometer 2). (×) (I) with no post-treatment; (○) (II) standard post-treatment under (1273 K, vacuum, 2 h); (●) (III) post-treatment under nitrogen (1273 K, 1.33 kPa, 1000 $cm^3 min^{-1}$, 2 h); (□) (IV) post-treatment under hydrogen (1273 K, 1.33 kPa, 1000 $cm^3 min^{-1}$, 2 h); (■) (V) post-treatment under ammonia (1273 K, 1.33 kPa, 1000 $cm^3 min^{-1}$, 2 h); (▲) (VI) high-temperature post-treatment (1473 K, vacuum, 2 h).

BN film has become partially unstuck and broken into many fragments (Fig. 13b). After ammonia post-treatment (V), the BN films are not completely broken and appear like large sheets partially unstuck from the carbon fibre (Fig. 13c). Following post-treatment at high temperature (VI), the BN films do not seem to be significantly damaged (Fig. 13d).

4. Discussion

4.1. Microstructure of the BN films prepared under standard conditions

The microstructure is discussed based on the results of Section 3.1.3 and of previous studies of CVD of BN. On the one hand, the occurrence of (i) a broad halo attributable to the X-ray reflection of the $d_{0\,0\,2}$ planes, slightly shifted to large inter-reticular distances, (ii) the two typical infrared vibrational modes (1390 and 790 cm^{-1} corresponding, respectively, to B–N stretching and B–N–B bending), and (iii) the typical Raman vibrational mode (1375 cm^{-1} corresponding to B–N stretching); all three results allow verification that the BN films are not totally amorphous, and contain crystallites with a network of B_3N_3 hexagons. On the other hand, the relatively weak intensities of all these data and the absence of the (1 0) reflection in the X-ray pattern shows that the ordering between boron and nitrogen atoms is limited to very small distances (nearly 1.5 nm, i.e. a stack of five or six (0 0 2) planes).

The BN density appears particularly low compared to its theoretical value (1.4 $g cm^{-3}$ instead of 2.27 $g cm^{-3}$). This is due firstly to the greater distance between the $d_{0\,0\,2}$ planes (0.36 nm instead of 0.333 nm) which leads to a density of 2.1 $g cm^{-3}$ for the BN crystallites, and second to an internal porosity of 33%. These two aspects are those classically encountered in BN films obtained by CVD at moderate temperature which have a similar microstructure to the CVD carbon deposits [10–12, 31, 32]; from the literature, it is assumed that the internal pores were microvoids of about 10 nm.

Finally, when compared to those reported in previous studies, our BN films are among the lowest ordered materials, which is consistent with the low deposition temperature (773 K), even if they are always post-treated at 1273 K [10–12, 31, 32].

4.2. The origin of oxygen contamination

Several recent studies showed that the CVD BN films sometimes contain a significant oxygen content, whose origin is not clearly identified [10–12]. From the results of Section 3, a more complete explanation may be proposed.

The XPS analyses performed on the BN/Si materials clearly show that the films already contain oxygen before their exposure to air (Table IX); therefore, part of the oxygen contamination originates from the CVI

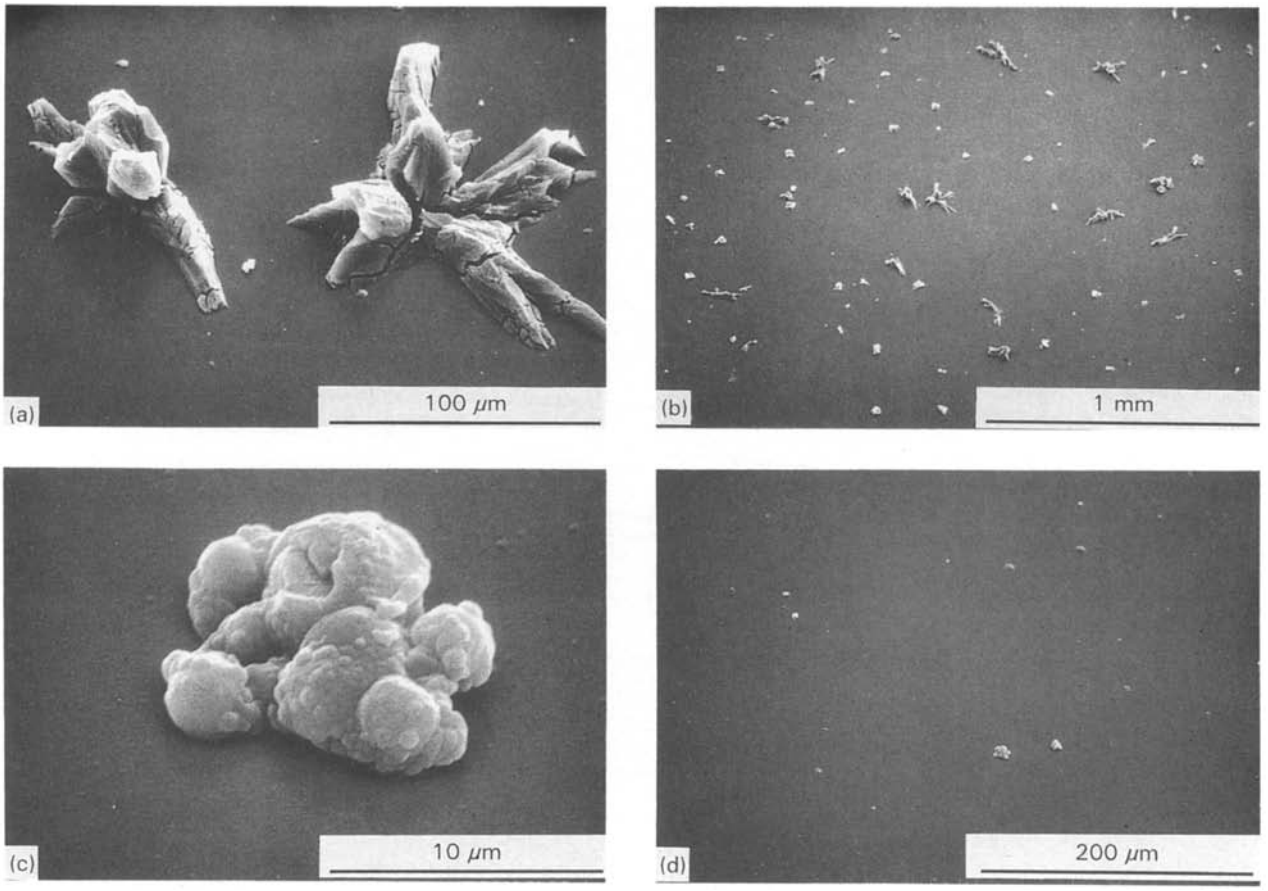

Figure 12 Morphological aspects of the BN films deposited on the silicon wafers: (a, b) with no post-treatment and after 300 h in air, (c, d) with no post-treatment and with a limited air exposure.

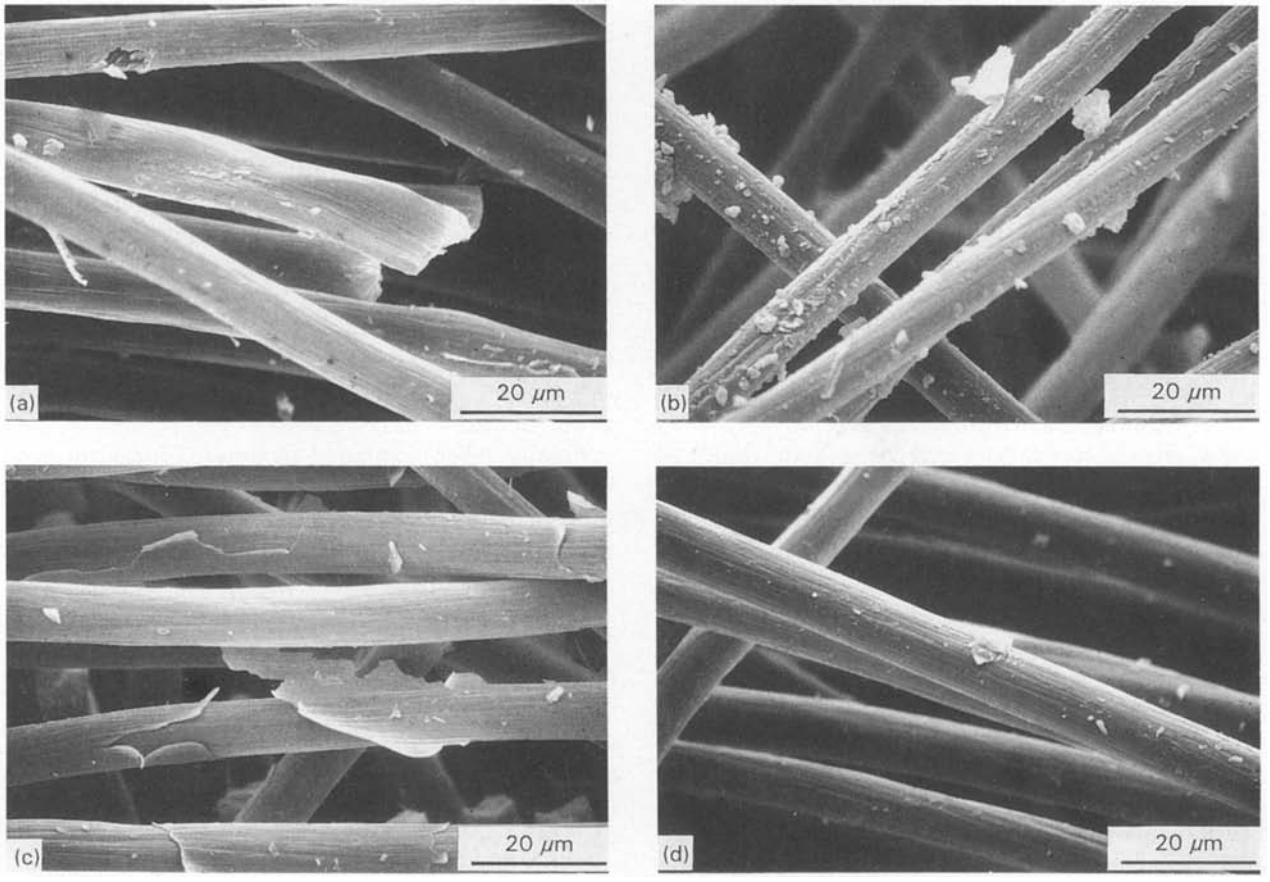

Figure 13 Morphological aspects of the BN layers deposited on the fibres of the fibrous preform after ageing and for the six post-treatments, both as defined in the text: (a) after post-treatment (I), (b) after post-treatments (II), (III) and (IV), (c) after post-treatment (V), (d) after post-treatment (VI).

step. Moreover, it was noticed in Section 2 that the CVD of the BCl_3–NH_3 mixtures produces some intermediate solids (probably boron amide and imide) which are highly hygroscopic. It was experimentally verified that these solid by-products absorbed a significant water content when the CVI reactor was opened for the introduction or removal of the substrates for coating; moreover their XPS analysis by spectrometer 1 (reported in Table XI) shows a large oxygen content, although most of the absorbed water is evaporated by the high dynamic vacuum inside the spectrometer (nearly 10^{-6} Pa). Consequently, it is proposed that these solid by-products act as a water source, which leads to a competition between the following reactions during the deposition step as water is liberated by the next temperature increase during the subsequent deposition experiment

$$BCl_3 + NH_3 \rightarrow BN + 3\,HCl \quad (1)$$

$$BCl_3 + 3/2\,H_2O \rightarrow 1/2\,B_2O_3 + 3\,HCl \quad (2)$$

TABLE XI Nature, binding energies and content of the chemical bonds detected on the intermediate solids analysed by XPS spectrometer 1

Chemical bond	Binding energy (eV)	Content (%)
B–N	190.3	72
B–O	192.4	25
B–Cl	193.5	3
N–B	397.7	91
N–?	399.6	9
O	532.2	100
$Cl_{2p\ 1/2}$	197.8	63
$Cl_{2p\ 3/2}$	199.5	37
O/B	–	48
N/B	–	83
Cl/B	–	3

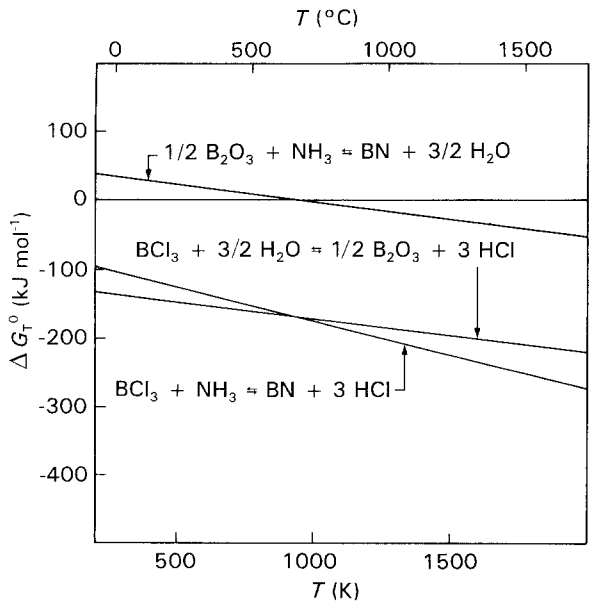

Figure 14 Variations of the standard free energy of the reaction between BCl_3 and NH_3, BCl_3 and H_2O, and the reaction representing the quasi-equilibrium between BN and B_2O_3 (thermodynamic data from [31]).

The variations of standard free energies as a function of temperature are reported in Fig. 14 from Janaf thermodynamical data [33]. It appears that a quasi-equilibrium can be maintained over a large temperature range, and a transition occurs at nearly 940 K (below 940 K, oxidation is promoted; above 940 K, nitridation is promoted); in fact, this situation corresponds to the following quasi-equilibrium between nitriding and oxidation of boron (Fig. 14)

$$1/2\,B_2O_3 + NH_3 \rightarrow BN + 3/2\,H_2O \quad (3)$$

which is independent of the type of boron precursor (B_2H_6, $B_3N_3H_6$, BF_3). This hypothesis appears to be confirmed by two sets of experimental results: (i) at 773 K, low total flow rates and low NH_3 flow rate (where a large part of the precursors is converted to amide and imide of boron [24]), the chemical reaction can be strongly displaced towards the oxidation side and then results in BN films which are characterized by B–O values higher than 30% (Class C, Table IV), (ii) at higher temperature (1073–1173 K), reactions 1–3 can be displaced towards the nitriding side, which then results in BN films which are characterized by B–O values lower than 10% (Class B, Table IV).

In addition to this oxygen content, the presence of further oxygen is clearly due to the action of moisture on the BN films when they are prepared by CVD from BCl_3–NH_3 mixtures (this study and [11, 12]) while it is not reported in the case of CVD from the BF_3–NH_3 mixtures [10].

The distinction between two origins of the oxygen content allows the question of oxygen distribution in the thickness of the BN films to be debated; Lacrambe [11] reported a high oxygen gradient from the external surface to the bulk BN, while Dugne [10] reported a homogeneous oxygen distribution inside the BN films. In fact, it is logical to think that (i) the initial oxygen content is due to the CVI process which leads to a homogeneous oxygen distribution over the whole BN thickness, and (ii) the remaining oxygen content is due to the external action of moisture, leading to a high oxygen gradient in the BN thickness, although this gradient should be reduced when the BN films have a high porosity, which favours diffusion of water in the films. Finally, in our case where the porosity is very high, the surface XPS analyses can be interpreted as fairly characteristic of the bulk BN, even if a slight gradient exists.

XPS analyses also revealed four different chemical states for the boron atoms (Table XII) which, with respect to the XPS accuracy ($\pm$ 0.2 eV), can be related to the origins of the oxygen and may be discussed in

TABLE XII The three different chemical states of the boron atoms encountered in the BN films from this study and other work [10, 11, 26]

Chemical bond	[10]	[11]	Spec. 1	Spec. 2
B–N (eV)	190.6	190.6	190.5	190.2
B–O (1) (eV)	191.9	–	–	191.8
B–O (2) (eV)	–	192.5	192.6	–

relation to the previous XPS investigations of CVD BN deposits [10, 11, 26] and the XPS analysis of our B_2O_3 reference (Merck): (i) an elemental peak at 190.4 eV corresponding to the hexagonal BN configuration where the boron nearest neighbours are three nitrogen atoms, (ii) an elemental peak at 193.5 eV corresponding to the hexagonal B_2O_3 configuration where the boron nearest neighbours are three oxygen atoms (B_2O_3 (Merck) and [10]), (iii) a first intermediate elemental peak at 191.8 eV, probably corresponding to a hexagonal configuration where boron is surrounded by two nitrogen atoms and one oxygen atom, and (iv) a second intermediate elemental peak at 192.6 eV, probably corresponding to a hexagonal configuration where boron is surrounded by one nitrogen atom and two oxygen atoms. In terms of destabilization, it is well correlated that (i) the detection of the boron binding energy at 191.8 eV is related to a low destabilization (the BN mass increases remain low and the growing crystals stay very small), (ii) the detection of the boron XPS peak at 192.5 eV is related to a high destabilization (reported on the BN/Si material which was not post-treated but exposed to air 300 h, and on the BN/C materials exposed for a very long time in air).

4.3. Incorporation of oxygen into the BN structure

The incorporation of the oxygen previously detected in the BN lattice (Fig. 15a) necessitates some structural modifications. The substitution of one nitrogen atom by one oxygen atom creates one dangling bond on the neighbouring boron atoms (Fig. 15b); on the other hand, the value of (O + N)/B, which is always higher than 1, can be taken as evidence of vacancies on the boron positions, as already reported by Lacrambe [11]; this situation clearly induces dangling bonds on the neighbouring nitrogen atoms (Fig. 15c). These two kinds of dangling bonds are obviously very unstable, and their existence in the BN films is improbable, especially when they are heated at 1273 K for 2 h; however, their structural accommodation remains an open question. Nevertheless, taking into account the presence of water vapour during both deposition and post-treatment and boron's great affinity for oxygen, some schemes can be submitted: (i) the addition of one water molecule allows the formation of one B–OH bond and one N–H bond while the two other dangling bonds associate themselves to form N–N bonds (Fig. 16a), (ii) because the pre-existing B–O bond is probably due to oxidation via one water molecule, two hydrogen atoms are available for bonding; when associated with another water molecule, they can form one B–OH bond and three N–H bonds (Fig. 16b), (iii) if the two types of punctual defects are close in the lattice, the insertion of one water molecule in the local void allows dangling bonds to be avoided (Fig. 16c). In every case, local deformation of the hexagonal BN lattice is necessary to accommodate these new chemical bonds, themselves being probably also slightly deformed. Obviously, these propositions necessitate other experimental data, but they show that the surroundings of the nitrogen are necessarily modified, in addition to that of boron. Moreover, the modification of the surroundings of both boron and nitrogen is clearly evident when the B–O terms reach high values; at B–O = 34%, the N–? content can reach an average of 21% (Table V). On the other hand, XPS analysis of ammonium borate hydrate $(NH_4)_2O \cdot 2B_2O_3 \cdot 4H_2O$ produces one peak at 400.0 eV, i.e. at the same binding energy as N–?; moreover, boron and oxygen are detected at 192.6 and 531.9 eV, respectively, i.e. at energies similar than those measured on BN films exposed to air for a long time.

4.4. Action of moisture on the BN materials

First, it is useful to note that the preliminary study (Section 3.2.1) showed the beneficial effect on the stability of BN of a high deposition temperature, to post-treat the coating and to limit the exposure time in air. On the other hand, as stated in Section 4.2, the

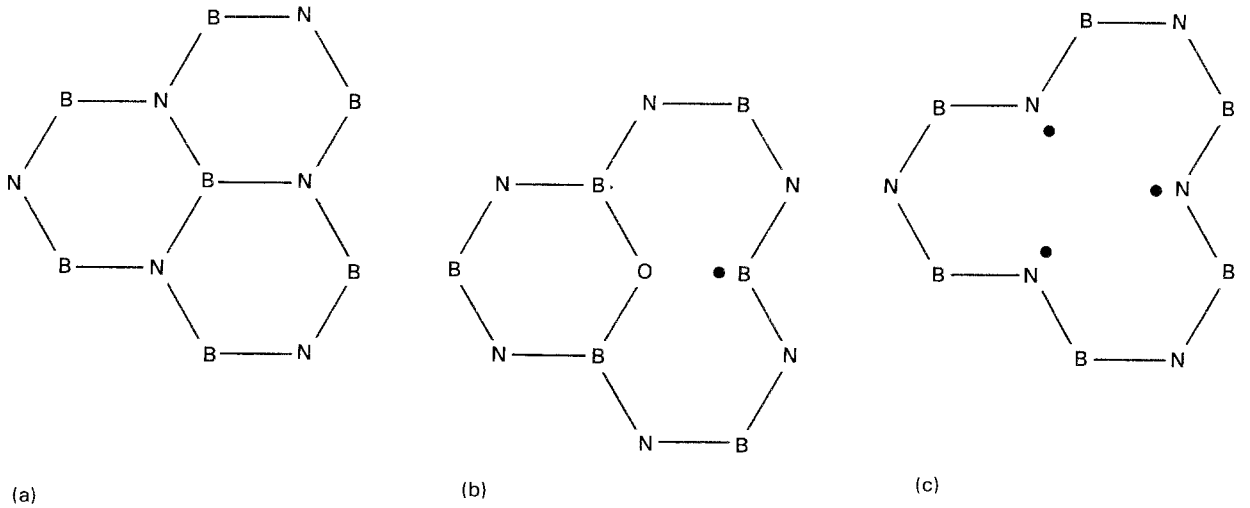

Figure 15 Schematic representation of the formation of dangling bonds via substitution of a nitrogen atom by an oxygen atom, and via the creation of boron vacancy.

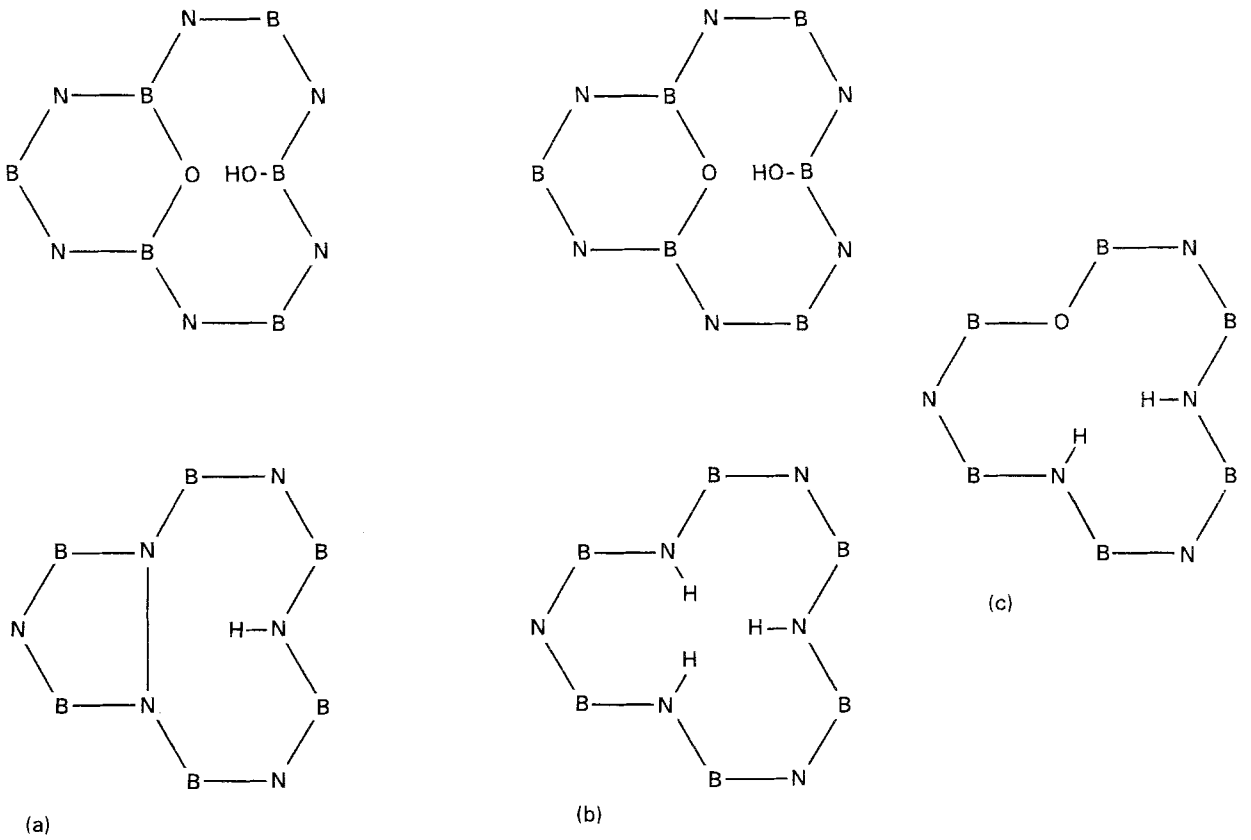

Figure 16 Schematic representation of hypothetical structural modifications accommodating the dangling bonds.

moisture action leads to a variation of the XPS boron spectra, the individual peak at 191.5 eV is replaced by another one at 192.5 eV, which appears to be correlated to the change from a moderate BN mass increase to a higher one, and is followed by the growth of white crystals.

However, these crystals cannot be H_3BO_3 crystals (Fig. 8) because, as seen in Section 4.3, the substitution of nitrogen by oxygen as nearest neighbours of boron also affects the nitrogen atoms, and then they are more probably ammonium borate hydrates. Because the micro-Raman spectroscopy showed that they are not exactly $(NH_4)_2O \cdot 2B_2O_3 \cdot 4H_2O$ (Fig. 7), they probably consist of $(NH_4)_2O \cdot 5B_2O_3 \cdot 8H_2O$ because (i) this compound was identified via IR spectroscopy by Matsuda [12] and also by Lacrambe [11] even though he does not emphasize this result (Fig. 17 shows the IR spectra recorded on the destabilized BN powders reported by these two authors), (ii) this compound has a very large nitrogen deficiency, compared to the BN stoichiometry, which can be explained by the formation of an NH_3 volatile product, whose smell is detected, during the destabilization at air, while the hydrolysis of the boron atoms leads to solid products. This last point is correlated with the lower values of N–? compared to those of B–O.

As noted before, a post-treatment after the CVI step strongly improves BN stability; this effect and those provided by the different types of post-treatments can be explained by taking into account the water vapour pressure. Actually, this improvement is probably related to the reduction of the total dangling bonds content, at the same time on boron and nitrogen atoms (via the mechanisms presented in Section 4.3, or other mechanisms to be discovered), because the water vapour pressure must be higher at 1273 K than at 773 K, if the water source is still efficient. The lower oxygen content recorded on the BN/Si material not post-treated and unexposed to air in comparison with the sample treated under standard post-treatment and also unexposed to air shows the occurrence of this oxidation during the standard post-treatment (I).

Compared to the standard post-treatment, post-treatment (II) under nitrogen appears identical and show that molecular nitrogen has no chemical effect on the BN stabilization at 1273 K. The post-treatment under hydrogen leads to a very similar stabilization; the very slightly higher BN mass variations and B–N values could originate from the formation of B–H bonds in addition to the B–OH bonds, as reported for H_2 annealing of non-stoichiometric BN films [34]; this association leads to some unlocated charge effect. The better stabilization by the post-treatment under ammonia clearly results from the nitriding of the B–O bonds which is favoured in comparison with the oxidation at 1273 K; this nitriding would be greatly improved at higher ammonia pressure because it was devised for the nitriding of the B_2O_3 fibres [2]. The apparent better stabilization obtained at 1473 K is probably related to the consumption of the deposit due to the volatilization of boron oxide, which becomes very efficient at temperatures higher than 1273 K, especially in the presence of water vapour, as reported by McKee [35].

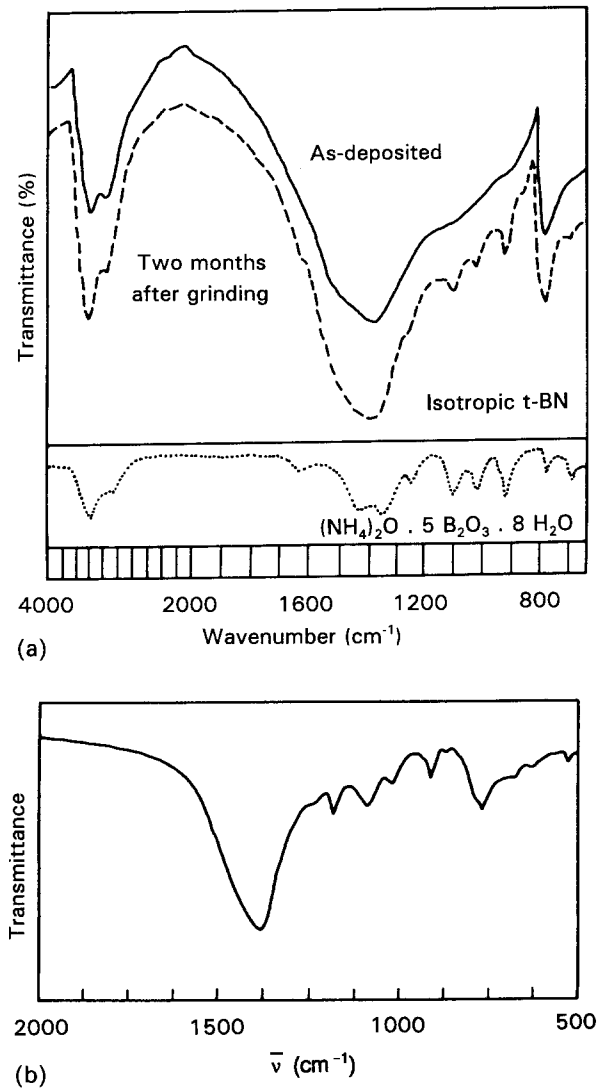

Figure 17 IR spectra of the destabilized BN powders: (a) spectrum reported by Matsuda [12] exhibiting the presence of $(NH_4)_2O \cdot 5B_2O_3 \cdot 8H_2O$, (b) spectrum recorded by Lacrambe [11].

The heating occurring after exposure to air, which simulates the heating occurring before the densification of the BN-coated preforms, has very drastic effects. The associated large BN mass decrease is clearly due, on the one hand, to the evaporation of the adsorbed water (nearly 75% of the total BN mass variation from Table VII), and on the other, probably to the volatilization of NH_3 and H_2O produced from the thermal decomposition of the ammonium borate hydrates and the partial volatilization of the resulting borate glass. Then, as function of the exposure time in air, the BN mass increases or decreases (Tables VI and VII).

5. Conclusions

The BN films prepared by CVD from BCl_3–NH_3–H_2 mixtures inside fibrous preforms are poorly organized materials, contaminated by oxygen and unstable in the presence of moisture. These characteristics are related to the low deposition temperature, which is necessary to obtain uniform high thicknesses inside the preforms, although the BN-coated preforms are post-treated at high temperature.

As-deposited, i.e. deposited, at 773 K and post-treated at 1273 K under a dynamic vacuum, the BN films are turbostractic and exhibit high d_{002} interlayer spacing, very small crystallites and very low density, and contain oxygen. This oxygen contamination has two different origins which can be distinguished by the resolution of the XPS boron spectrum. One part of the oxygen, corresponding to an individual peak at 191.5 eV ($\pm$ 0.2 eV), emanates from the water vapour released by the intermediate solids formed before the deposition zone. The oxygen incorporation in the BN films is favoured by the quasi-equilibrium between BN, B_2O_3, NH_3 and H_2O which extends over a large temperature range, and also by the low deposition temperature placed on the oxidation side of this equilibrium. This evidence is related to a low BN stability in the presence of moisture. The second part of oxygen, corresponding to an individual peak at 192.5 eV ($\pm$ 0.2 eV), originates from the action of moisture upon exposure to air, which leads to important BN mass increases and to the growth of "destabilization crystals". These crystals consist of ammonium borate hydrates, and more probably of $(NH_4)_2O \cdot 5B_2O_3 \cdot 8H_2O$.

However, the incorporation of oxygen induces some modifications in the BN hexagonal structure which lead to a second individual XPS peak for N_{1s} at 399.5 eV, probably corresponding to N–H or N–N bonds.

As a function of the exposure time in air, the boron XPS peak at 191.5 eV is replaced by one at 192.5 eV, and a drastic destabilization occurs. This BN instability can be reduced by (i) a nitriding post-treatment under ammonia, (ii) an increase of the deposition temperature (although the uniformity of thickness in the preform will decrease), (iii) the deposition of a stable material on BN, and (iv) control of the water vapour pressure and an adapted pre-treatment prior to the CVI step.

Acknowledgements

The authors thank Dr P. Echegut, Dr C. Beny and Mr Simonato, for IR investigations, Raman investigations and SEM investigations, respectively, Mrs R. Herbin for her contribution to the preparation of the manuscript, and Mr Carlino for his contribution in the design and construction of the CVI reactor. This work was supported by the Societe Europeenne De Propulsion and the authors thank especially Drs Rey and Robin–Brosse for their assistance. This was part of the thesis of V. Cholet (Orléans – 25 April 1990) granted by SEP.

References

1. S. P. S. ARYA and A. D'AMICO, *Thin Solid Films* **157** (1988) 267.
2. J. ECONOMY and R. LIN, "Boron and Refractory Borides" (Springer, Berlin, 1977) p. 552.
3. M. J. RAND and J. F. ROBERTS, *J. Electrochem. Soc.* **115** (1968) 423.
4. A. C. ADAMS and C. D. CAPIO, *ibid.* **127** (1980) 399.
5. A. C. ADAMS, *ibid.* **128** (1981) 1378.

6. T. MATSUDA, N. UNO, H. NAKAE and T. HIRAI, *J. Mater. Sci.* **21** (1986) 649.
7. J. M. L. MARTIN, J. P. FRANCOIS and R. GIJBELS, in "Proceedings of the 7th European Conference on CVD", Perpignan, France, edited by C. Bernard Ducarroir and L. Vandenbulcke (Editions Physiques, Paris, 1989) p. 833.
8. H. O. PIERSON, *J. Compos. Mater.* **9** (1975) 228.
9. H. HANNACHE, Thesis no 813, Bordeaux University (1984).
10. O. DUGNE, Thesis no 375, Bordeaux University (1989).
11. G. LACRAMBE, Thesis no 2232, Bordeaux University (1988).
12. T. MATSUDA, *J. Mater. Sci.* **24** (1989) 2353.
13. K. M. PREWO and J. J. BRENNAN, *ibid.* **15** (1980) 463.
14. *Idem, ibid.* **17** (1982) 1201.
15. J. J. BRENNAN and K. M. BRENNAN, *ibid.* **17** (1982) 2371.
16. J. J. BRENNAN, "Tailoring Multiphase and Composite Ceramics", Vol. 20 (Plenum, New York, 1985) p. 549.
17. M. H. RAWLINS, T. A. NOLAN, D. P. STINTON and R. A. LOWDEN, *Mater. Res. Soc. Symp. Proc.* **78** (1986) p. 223.
18. J. G. THEBAULT, Fr. Pat. 2567 874, 20 July, 1984.
19. L. GRATEAU, Thesis no 779, Orsay University (1987).
20. R. W. RICE, US Pat. 4642 271, 10 February 1987.
21. R. N. SINGH and M. K. BRUN, *Adv. Ceram. Mater.* **3** (1988) 235.
22. B. BENDER, A. SHADWELL, C. BULIK, L. INCOVARTI and D. LEWIS, *Am. Ceram. Soc. Bull.* **65** (1986) 363.
23. D. P. STINTON, A. J. CAPUTO and R. A. LOWDEN, *ibid.* **65** (1986) 347.
24. V. CHOLET and L. VANDENBULCKE, *J. Am. Ceram. Soc.* **76** (1993) 2846.
25. R. N. SINGH, in "Proceedings of the 10th International Conference on CVD", Honolulu, edited by G. W. Cullen (The Electrochemical Society, Pennington, NJ, 1987) p. 543.
26. G. B. FREEMAN, W. J. LACKEY and T. L. STARR, in "Proceedings of the 46th Annual Meeting of the Electron Microscopy Society of America", edited by G. B. Bailey (San Francisco Press, Atlanta, 1988) p. 740.
27. C.D. WAGNER, in the "Handbook of X-ray Photoelectron Spectroscopy", edited by G. E. Mullenberg (Perkin Elmer, Eden Prairie, MN, 1978) pp. 35, 40.
28. B. D. CULLITY, "Elements of X-rays Diffraction" (Addison Wesley, London, 1967).
29. R. J. NEMANICH, S. A. SOLIN and R. M. MARTIN, *Phys. Rev. B*, **23** (1981) 6348.
30. T. MATSUDA, H. NAKAE and T. HIRAI, *J. Mater. Sci.* **23** (1988) 509.
31. J. ECONOMY and R. V. ANDERSON, *J. Polym. Sci. C* **19** (1967) 283.
32. T. E. O'CONNOR, US Pat. 3241 919 (1966).
33. "Janaf Thermochemical Tables", 3rd Edn edited by M. W. Chase Jr., C. A. Davies, J. R. Downey Jr., D. J. Frurip, R. A. McDonald and A. N. Syverud (American Chemical Society and American Institute of Physics, Midland, MI, 1985).
34. R. A. LEVY, in "Proceedings of the 1st International Conference on Diamond Films", Los Angeles, edited by J. P. Dismukes, A. J. Purdes, B. S. Meyerson, T. D. Moustakas, K. E. Spear, K. V. Ravi and M. Yoder (The Electrochemical Society, Pennington, NJ, 1989) p. 182.
35. D. W. McKEE, *Carbon* **25** (1986) 737.

Received 21 July 1992
and accepted 31 August 1993